Condensation phase diagram of cavity polaritons in GaN-based microcavities: Experiment and theory

Jacques Levrat, Raphaël Butté, Eric Feltin, Jean-François Carlin, and Nicolas Grandjean
Institute of Condensed Matter Physics, École Polytechnique Fédérale de Lausanne (EPFL), CH-1015 Lausanne, Switzerland

Dmitry Solnyshkov and Guillaume Malpuech
LASMEA, Clermont Université–Université Blaise Pascal, BP 10448, 63000 Clermont-Ferrand, France
and UMR 6602, LASMEA, CNRS, 63177 Aubière, France

(Received 1 December 2009; revised manuscript received 8 February 2010; published 5 March 2010)

The evolution of the polariton condensation threshold (P_{thr}) under incoherent optical pumping is investigated both theoretically and experimentally over a wide range of temperatures (4–340 K) and exciton-cavity photon detunings (−120–0 meV) in a multiple quantum-well GaN-based microcavity. The condensation phase diagram of these bosonic quasiparticles is first theoretically described within the framework of Bose-Einstein condensation of polaritons in the thermodynamic limit. Then a qualitative picture of cavity polariton relaxation kinetics including the impact of detuning and temperature is given before introducing a modeling of cavity polariton relaxation kinetics with semiclassical Boltzmann equations. The results of the theoretical modeling are finally compared with systematic measurements of P_{thr}. At low temperature and negative detunings, the polariton gas is far from thermal equilibrium and the condensation threshold is governed by the efficiency of the relaxation kinetics of the particles. Conversely, at high temperature and for less negative detunings, the relaxation kinetics is efficient enough to allow the achievement of a thermal polariton distribution function with a critical density for condensation given by the thermodynamic theory of Bose-Einstein condensation. For temperatures ranging between ~140 and 340 K, an optimum detuning is found experimentally, where the condensation threshold power is minimized. At high temperatures, polariton detrapping effects from the bottom of the trap formed in $k_{\|}$ space by the lower polariton branch are found to play a supplementary role among the processes governing P_{thr}.

DOI: 10.1103/PhysRevB.81.125305 PACS number(s): 71.36.+c, 03.75.Nt, 78.67.De, 42.55.Sa

I. INTRODUCTION

The peculiar physical properties of interacting Bose gases and liquids in three dimensions (3D) and two dimensions (2D) have triggered many theoretical[1–5] and experimental[6,7] studies during the past century. Many of these studies were first devoted to liquid helium and the superfluid behavior that may arise in such a system. In recent years, several other systems have been considered to investigate the occurrence of bosonic condensation phenomena in the solid state. Such phenomena have thus been reported with magnons,[8,9] which are the elementary quanta of spin waves in ordered magnetic materials, and cavity polaritons in planar semiconductor microcavities (MCs),[10–13] which are the quasiparticles resulting from the strong coupling of excitons and cavity photons.

In the present work, we will focus on the latter type of system with a more specific emphasis on the conditions leading to polariton condensation which has recently been reported at room temperature (RT) in multiple quantum well (MQW) GaN-based MCs.[13] Note that by polariton condensation we encompass both the notion of polariton lasing and Bose-Einstein condensation (BEC) of polaritons, as already discussed by Kasprzak and co-workers[14] and as will be discussed further below.

It is also worth pointing out the main differences between a polariton laser and a vertical cavity surface-emitting laser (VCSEL), the photon laser the closest to a polariton laser. Both types of structures rely on a planar semiconductor MC geometry and the active medium can be either a bulk semiconductor, or it might contain quantum wells or even quantum dots.[15] For VCSELs, as in any conventional laser, an external pumping, optical or electrical, drives the electron-hole distribution out of equilibrium, which results in photon emission into the cavity mode. The lasing threshold is then reached provided two conditions are fulfilled. First, inversion of the electron-hole distribution should be obtained for the system to exhibit net stimulated photon emission, which also means that the emission of light should be stronger than the absorption process. This is the case when the Bernard-Durrafourg condition is fulfilled.[16] In this situation, the system operates in the weak-coupling regime, where emitted photons result from the spontaneous or stimulated recombination of electron-hole pairs. The second condition to be fulfilled for the lasing threshold to be passed is that the gain in the active region should be increased up to values such that propagation and mirror losses are compensated to get an effective optical feedback leading to lasing oscillations. One of the main advantages of VCSELs over standard edge-emitting lasers is that the cavity mode exhibits a much higher-quality factor $Q(=\lambda/\Delta\lambda)$ allowing a reduction in the lasing threshold by several orders of magnitude. This is also due to the fact that such vertical cavity laser structures are usually characterized by a much larger spontaneous emission coupling factor β, i.e., a larger coupling efficiency of spontaneous emission into the lasing mode (assuming we consider a single-frequency laser), than their edge-emitting counterparts.[17] The next step to further reduce the lasing threshold is to minimize or even cancel the first constraint

(the gain condition). This can be achieved in planar semiconductor MCs by working in the strong-coupling regime (SCR).[18] The achievement of this regime requires a large excitonic absorption peaked in a sufficiently narrow energy range, in addition to a high-Q factor. The new eigenmodes of the system are the so-called cavity polaritons.[15] At small and medium densities, polaritons are expected to behave as weakly interacting bosons and should be able to undergo a bosonic phase transition toward a condensate. If such a phase transition takes place, a macroscopic polariton population will *a priori* accumulate in the ground state. In that case, polariton relaxation is governed by scattering processes stimulated by final-state occupation, and the spontaneous radiative decay of these short-lived particles (in the picosecond range) leads to a coherent emission of photons without requiring population inversion. Such a system, first proposed in 1996,[19] has been called a polariton laser. From a fundamental point of view, this proposal attracted a lot of interest since it shares many similarities with Bose-Einstein condensation, an effect very actively sought for in solid-state systems during half a century.[10] The motivation behind the realization of polariton lasers is therefore both scientific and technological. The first clear experimental evidence of the bosonic behavior of cavity polaritons and of their capacity to undergo stimulated scattering has been reported in 1998 under nonresonant excitation[20] and in 2000 under resonant excitation.[21] Evidence for polariton BEC and polariton lasing has then been reported first at low temperature in both CdTe and GaAs microcavities.[10,11,22] The realization of devices however requires achieving polariton condensation at RT which implies the use of wide band-gap semiconductors showing simultaneously RT stable excitons and a very large exciton-photon coupling strength. GaN (Ref. 23) and ZnO (Ref. 24) have therefore been proposed as excellent candidates for the realization of RT polariton lasers. If we focus on the more advanced GaN-based MC structures, samples with a bulk active region have been first considered due to their simpler geometry and ease of fabrication compared with heterostructure-based active regions to achieve the SCR at RT.[25,26] Polariton lasing[12] and polariton BEC (Ref. 27) occurring at RT have then been reported in such a sample. The second generation of samples currently involves the use of appropriately designed GaN MQWs owing to their larger exciton oscillator strength, larger exciton binding energy, and hence their larger exciton saturation density compared with bulk systems.[28] It allowed improving the polariton lasing threshold conditions with respect to bulk samples[13] by 1 order of magnitude, as it was predicted theoretically.[29] The actual threshold depends on how far the polariton gas is from quasithermal equilibrium, which, in turn, is dictated at first sight by the ratio between the polariton relaxation time and the mean polariton lifetime. The absolute constraint for a polariton laser to work is therefore the achievement of fast enough relaxation kinetics for polaritons injected nonresonantly by an external pumping source.

In this framework, it is essential to achieve a good understanding of the main parameters governing the polariton condensation threshold (P_{thr}). In particular, it has been recently evidenced that the exciton-photon detuning δ (Ref. 30) and the temperature are essential parameters controlling this threshold.[14,31,32] Consequently in the present paper, following a brief description of the microcavity sample and experimental details (Sec. II), we provide a theoretical picture of cavity polariton condensation applied to the case of the GaN-MQW microcavity described in Refs. 13 and 28, first by considering BEC of polaritons in the thermodynamic limit (Sec. III A). Then, a qualitative picture of cavity polariton relaxation kinetics including the impact of detuning and temperature is given (Sec. III B) before introducing a modeling of cavity polariton relaxation kinetics with semiclassical Boltzmann equations (Sec. III C). The results of the theoretical modeling are compared with systematic measurements of P_{thr} performed on the above-mentioned GaN-MQW microcavity (Sec. IV) and eventually the main conclusions are summarized (Sec. V).

The results reported are complementary to the distinctive features known so far for polariton lasers with respect to conventional lasers, namely, the continuous blueshift and the increase in the linewidth of the condensate emission due to polariton-polariton interactions above threshold with increasing pumping power[10–13,33] or the behavior of the second-order time-correlation function.[34]

II. SAMPLE DESCRIPTION AND EXPERIMENTAL DETAILS

The MC sample studied in this paper has been extensively described elsewhere.[13,28] However, its main features are summarized in this section. It is a crack-free hybrid structure which consists of a high reflectivity bottom epitaxial 35 pair lattice-matched $Al_{0.85}In_{0.15}N/Al_{0.2}Ga_{0.8}N$ distributed Bragg reflector (DBR) followed by a 67 period GaN (1.2 nm)/$Al_{0.2}Ga_{0.8}N$ (3.6 nm) MQW 3λ-cavity structure grown on (0001) sapphire substrate. A 67-nm-thick Si_3N_4 layer ($\sim 1.3\lambda/4$) has been inserted before a 13 pair top dielectric SiO_2/Si_3N_4 DBR in order to reach small negative detunings. Such a design ensures an optimum optical confinement for the lower polariton branch (LPB) and upper polariton branch (UPB) within the MC stop band. This latter point is further illustrated when considering the color maps of the computed RT angle-resolved reflectivity spectra of this structure ranging from 0° to 55° obtained using transfer-matrix simulations.[35] Calculations, accounting for the refractive index dispersion and absorption (including the contribution of Urbach tail and band-to-band absorption),[36] have been carried out for zero detuning and a negative detuning of −40 meV [Figs. 1(a) and 1(b), respectively]. The parameters considered here are the nominal thicknesses and a value of the oscillator strength f_{osc} of 4.5×10^{13} cm^{-2} to describe each QW. The refractive indices for III-nitride compounds are taken from the work of Brunner *et al.*[37] (AlGaN alloy) and Carlin *et al.*[38,39] (AlInN alloy). The optical properties of SiO_2 and Si_3N_4 layers were determined using thick layers grown on sapphire substrates. The normal-mode splitting Ω of 56 meV deduced from simulations for this structure does indeed correspond to that experimentally measured in the low carrier density regime.[13] This structure is characterized by an experimental Q factor slightly exceeding 1000, which leads to a cavity photon lifetime $\tau_c \sim 0.2$ ps. Such a GaN/

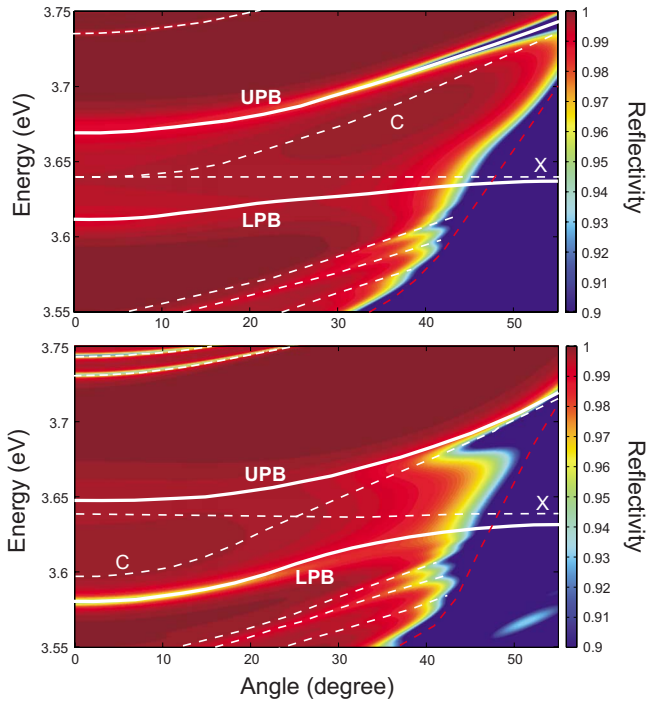

FIG. 1. (Color online) Color maps of the RT computed angle-resolved reflectivity spectra ranging from 0° to 55° for δ=0 meV (top) and δ=−40 meV (bottom). The polariton branches (LPB and UPB, thick white lines), the uncoupled exciton and the cavity mode (X and C, dashed white lines) as well as the first Bragg mode of the dielectric DBR (dashed red line), and the Bragg modes of the bottom nitride DBR (unlabelled dashed white lines) are reported.

AlGaN MQW system should exhibit a large exciton saturation density $\sim 1.3\times 10^{12}$ cm^{-2} per QW.[28] The suitability of this sample regarding the achievement of nonlinear effects associated with cavity polaritons was indeed recently confirmed by a clear signature of RT polariton lasing.[13]

Temperature-dependent angular-resolved photoluminescence (PL) measurements under nonresonant optical pumping were performed in reflection geometry using a two arm goniometer by means of a pulsed 266 nm (E_{laser}=4.66 eV) Nd:YAG laser with a repetition rate of 8.52 kHz and a pulse length of 500 ps, much longer than the polariton lifetime. The laser beam was focused down to a 50 μm diameter spot on the top dielectric DBR incident at a fixed angle of 45°. A continuous-flow liquid-helium cryostat allowed tuning the temperature from 4 to 340 K. The emitted light was then collected by a 400 μm core UV optical fiber using appropriate optics offering an angular selection of ±1° and detected by a liquid-nitrogen-cooled UV-enhanced charge-coupled device—monochromator combination with a spectral resolution of 150 μeV.

III. THEORETICAL DESCRIPTION OF CAVITY POLARITON CONDENSATION

A. Bose-Einstein condensation of cavity polaritons in the thermodynamic limit

Here, QW excitons are assimilated to weakly interacting bosons in the low to medium carrier density range so that in turn cavity polaritons also behave as weakly interacting bosons in the same density range. Polaritons are considered to interact with a phonon bath characterized by a lattice temperature T_{latt}. Furthermore, we assume in this section that the polariton lifetime is much longer than their typical relaxation time. This is indeed a prerequisite condition in order to reach an equilibrium with the lattice and thus the thermodynamic limit. Note that in the present experiments this thermodynamic limit represented by T_{latt} cannot be fully reached by photocreated carriers. One of the goals of this paper will therefore consist in quantifying the thermalization process to check whether a thermodynamic picture could apply to the polariton condensate in some regions of the phase diagram. Thermalization means that the polariton gas can be described by the Bose-Einstein distribution with a certain temperature. For some critical density if the system were ideal, the polariton gas should undergo a Kosterlitz-Thouless phase transition toward a superfluid state.[40] This type of phase transition is however strongly hindered by the presence of structural inhomogeneities. In that case, the polariton gas should first undergo a bosonic phase transition toward an Anderson glass,[41] before becoming superfluid at larger densities. Such a situation, originating from structural imperfections, cannot be presently avoided in III-nitride based samples which exhibit strong in-plane spatial photonic disorder.[42] The critical density for this phase transition to take place is defined as the total number of polaritons which can be accommodated in all the energy levels of the disorder potential except the ground one,[40,41]

$$n_c = \frac{1}{R^2}\int_{E_1}^{+\infty} \frac{g(E)}{\exp(E/k_BT)-1}dE, \qquad (1)$$

where R is the size of the lowest-energy trap seen by polaritons in the system, $g(E)$ is the 2D density of states (2D-DOS), E is the polariton energy, k_B is the Boltzmann constant, T is the temperature, E_1 is the energy of the first localized excited state, and the zero of energy is given by the position of the lowest-energy state.

Figure 2(a) shows the critical density $n_c(T_{latt})$ for different detunings. The vertical dashed line shows the critical temperature of the thermal dissociation of excitons ($T_{diss}\sim$560 K). The horizontal dashed line is the exciton/polariton density at which the exciton oscillator strength is expected to be bleached ($n_{sat}\sim 8.7\times 10^{13}$ cm^{-2}).[43] This density is close to the transparency limit and a VCSEL is expected to work only above this limit. As in any thermodynamic phase transition, the critical density increases versus T_{latt}. The dependence of $n_c(T_{latt})$ is however not linear on this log-log scale because of the nonparabolicity of the lower polariton branch. Another informative way to display the critical density consists in plotting $n_c(\delta)$ at various temperatures, as in Fig. 2(b) where the evolution of $n_c(\delta)$ is shown for three lattice temperatures (T_{latt}=40, 160, and 300 K). One can clearly observe that the more negative the detuning, the lower the critical density for polariton BEC. This is due to the decreasing 2D-DOS of the lowest-energy polariton state with increasing photon fraction. As an intermediate conclu-

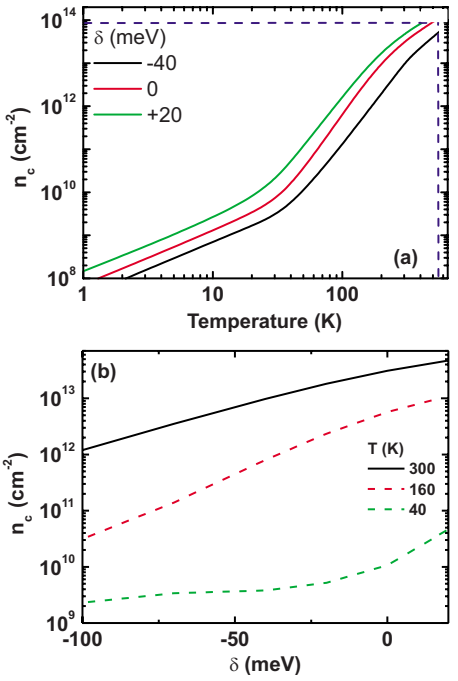

FIG. 2. (Color online) Critical density for polariton BEC in the thermodynamic limit: (a) as a function of temperature for different δ values and (b) as a function of δ for different temperatures. The dashed blue lines in (a) indicate the limits of the SCR fixed by the exciton/polariton screening density (horizontal line) and the exciton dissociation (vertical line).

sion, in the thermodynamic limit P_{thr} is expected to increase both with temperature and when going toward more positive detunings.

B. Qualitative picture of cavity polariton relaxation kinetics: Impact of detuning and temperature

As mentioned above, the previous description of condensation obviously holds for particles exhibiting a long (infinite) lifetime, as it allows the system reaching thermodynamic equilibrium. However, an inherent characteristic of cavity polaritons is their short lifetime close to $k_{\|}=0$ which is inherited from cavity photons.[44] Near the center of the Brillouin zone, i.e., in the central region of the dispersion, where the SCR holds, the inverse of the lower polariton lifetime is given in the first approximation by $\frac{1}{\tau_{pol}}=\frac{|C_L(k_{\|})|^2}{\tau_c}$, where $|C_L(k_{\|})|^2$ is the photon fraction of lower polaritons with in-plane wave vector $k_{\|}$. On the other hand, a dominant part of the dispersion curve corresponds to states with a wave vector larger than that of cavity photons. That part of the lower polariton branch is essentially an exciton reservoir, where excitons are not coupled to the light. Their lifetime is therefore given by the nonradiative exciton lifetime τ_{NR}. In a general way, the mean polariton gas lifetime reads

$$\frac{1}{\tau_{pol}}=\frac{\sum_{k_{\|}}(|C_L(k_{\|})|^2/\tau_c+|X_L(k_{\|})|^2/\tau_{NR})}{N}, \quad (2)$$

where $|X_L(k_{\|})|^2$ is the exciton fraction of lower polaritons with in-plane wave vector $k_{\|}$, $N=\Sigma_{k_{\|}}n_{k_{\|}}$ is the total number of particles in the system, and $n_{k_{\|}}$ is the occupation of the lower exciton-polariton state with a given wave vector $k_{\|}$. This occupation number can be deduced either from kinetic simulations or from the Bose distribution function, depending on the situation. In a typical experiment, electron-hole pairs are injected in the cavity via an optical or electrical pumping scheme. In the present experiment, where the nonresonant excitation photon energy lies well above the uncoupled exciton energy, these electron-hole pairs are expected to very rapidly bind to form excitons thanks to an efficient interaction with optical phonons.[45] Then these excitons thermalize to some effective temperature through exciton-exciton and exciton-phonon interactions. This thermalization process is usually quite efficient along the excitonic part of the dispersion and once the kinetic energy is less than the optical phonon energy, the whole exciton-polariton gas dissipates energy by interacting with the lattice by emitting acoustic phonons. In principle, the combination of these two complementary relaxation mechanisms is efficient enough to allow the polariton gas reaching a temperature close to the lattice temperature in the excitonic part of the dispersion.[46] In the central part of the Brillouin zone, also called "polariton trap" for lower polaritons, the above-mentioned relaxation mechanisms have to compete with the increasingly shorter radiative lifetime of polaritons and the steep dispersion which reduces the efficiency of the relaxation process through acoustic phonon scattering. This tendency, which manifests itself by a lack of particles in the trap region with respect to a thermal distribution and by their accumulation in the reservoir region above the trap is the so-called "relaxation bottleneck effect."[47] Though the suppression of this bottleneck effect has been reported in different MC systems,[10,11,27,48] an important parameter governing polariton condensation is the relaxation time τ_{rel} needed for the polariton gas to cool from some initial temperature given by the pumping to the lattice temperature. At first sight, this relaxation time will depend on both the MC structure parameters (such as the detuning) and on the polariton density because of the polariton-polariton interaction. τ_{rel} has thus been derived from kinetic simulations, as will be discussed in the next section. On the one hand, if $\tau_{rel}\ll\tau_{pol}$, a polariton distribution in reasonable equilibrium with the lattice should be observed and in this latter case, BEC of polaritons should occur at density values close to those predicted by the thermodynamic theory. On the other hand, if $\tau_{rel}\gg\tau_{pol}$, the polariton distribution is a nonequilibrium one, fully governed by the relaxation kinetics of particles. In the intermediate regime, both kinetic and thermodynamic aspects will play some role. Note again here that it is possible to play with both τ_{rel} and τ_{pol} through a change in δ, as sketched in Fig. 3(a). Indeed, the lifetime of lower polaritons is mainly inversely proportional to the photon fraction so that it increases when going from negative to positive values. Conversely, τ_{rel} decreases when going from negative to positive δ values due to the shallower polariton trap depth and the larger excitonic fraction of lower polaritons and the increased polariton-polariton and polariton-phonon interactions. From a kinetic point of view, it is therefore favorable to move toward positive detunings. On the other hand, as discussed in Sec. III A, from a thermodynamic point of view, the lowest values of the critical density n_c are

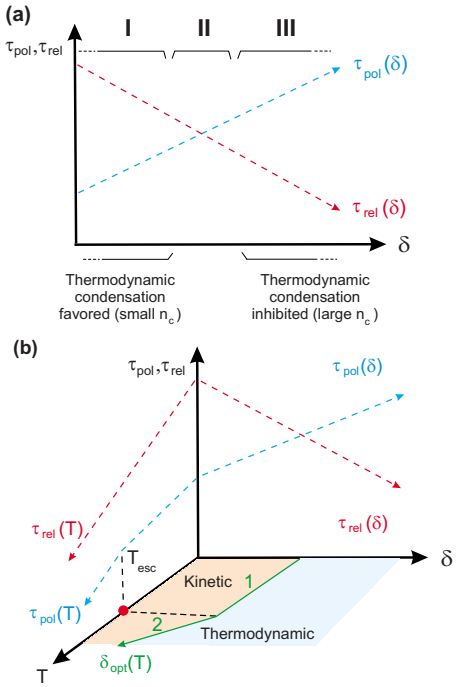

FIG. 3. (Color online) (a) Schematic description of the dependence of the mean polariton lifetime and the polariton relaxation lifetime under nonresonant excitation at a given cryogenic temperature as a function of detuning showing regions where either the kinetic condensation (region I) or the thermodynamic condensation (region III) or both relaxation regimes (region II) are favored (see text for details). (b) Refined qualitative diagram of the evolution of relevant lifetimes governing polariton condensation under nonresonant excitation as a function of either δ or T allowing defining the line $\delta_{opt}(T)$ leading to condensation which separates regions dominated by kinetics and thermodynamics (see text for details).

achieved when going toward negative detunings at all temperatures.

Note that at low cryogenic temperatures, as a first approximation in the 2D limit, n_c linearly depends on the polariton effective mass at the bottom of the trap (which is in fact strictly true for a parabolic trap only), which is itself an increasing function of δ. In terms of n_c, the thermodynamic condensation regime is thus expected to be favored for the smallest detunings.

The relevant parameters being defined, we can now focus on the expected evolution of $P_{thr}(\delta)$. In the kinetic regime [region I in Fig. 3(a)] at a given cryogenic temperature, the polariton relaxation is strongly inhibited due to the progressive decrease in their matterlike character with decreasing δ values, whereas n_c rapidly decreases. On the opposite, in the thermodynamic regime [region III in Fig. 3(a)], phonon-assisted relaxation is favored due to the increasing excitonic content of polaritons when going toward more positive detunings whereas a simultaneous increase in n_c occurs. As a result, the system must cope with opposite constraints in these two regions (I and III) so that an optimum situation is likely to occur in the intermediate regime where $\tau_{rel} \sim \tau_{pol}$ [region II in Fig. 3(a)]. This way, we can extract an optimum detuning δ_{opt} where the threshold power for condensation is minimized.

The occurrence of the three previously defined regimes and of an optimal detuning value have been reported in CdTe- and GaAs-based microcavities.[14,31] However, due to the narrow range of temperatures effectively explored, the plot of $\delta_{opt}(T)$ and that of the threshold power density for condensation versus T at $\delta_{opt}(T)$ were not shown. The advantage of the GaN-based system is that it allows accessing a very wide temperature range (4–340 K in the present work). When such a large variation in the lattice temperature (spanning 2 orders of magnitude) comes into play, the situation is expected to get somewhat more intricate. In particular, due to the significant increase in exciton-phonon and polariton-phonon interactions with increasing temperature, τ_{rel} should undergo a net decrease. On the other hand, the increase in the temperature should make higher the thermodynamic critical density leading to polariton condensation. The combination of these two effects should therefore shift δ_{opt} toward more negative detunings when the temperature rises. In addition, it has been recently shown that in the present MQW GaN-based MC, the buildup of polariton condensates is affected when the energy trap depth, formed in $k_\parallel$ space by the LPB, gets closer to the lattice temperature and thermal escape of polaritons from the bottom of the trap toward LPB states beyond the inflection point occurs (i.e., the nonparabolicity of the dispersion starts to influence the thermodynamic threshold density).[32] We should therefore expect to observe a critical escape temperature T_{esc} beyond which the optimum polariton condensation threshold will strongly increase due to a large depletion of the fundamental LP state. This strong depletion effect should be responsible for an enhanced shift of the optimum detuning for condensation toward more negative δ values. The occurrence of these cumulative effects is displayed in Fig. 3(b) showing the line $\delta_{opt}(T)$ leading to polariton condensation which separates regions dominated by kinetics and thermodynamics. Parts 1 and 2 of $\delta_{opt}(T)$ correspond to regions of weak and strong thermal escape of polaritons from the bottom of the energy trap, respectively.

C. Modeling of cavity polariton relaxation kinetics with semiclassical Boltzmann rate equations

Simulations of polariton relaxation are performed using semiclassical Boltzmann rate equations,[47]

$$\frac{dn_{k_\parallel}}{dt} = P_{k_\parallel} - \Gamma_{k_\parallel} n_{k_\parallel} - n_{k_\parallel} \sum_{k'_\parallel} W_{k_\parallel \to k'_\parallel} (n_{k'_\parallel} + 1) + (n_{k_\parallel} + 1) \sum_{k'_\parallel} W_{k'_\parallel \to k_\parallel} n_{k'_\parallel}, \quad (3)$$

where $n_{k_\parallel}$ is the occupation number of a state with in-plane wave vector $k_\parallel$, the $P_{k_\parallel}$ and $\Gamma_{k_\parallel}$ terms describe the pumping and decay rates of particles (including both radiative and nonradiative components), and $W_{k_\parallel \to k'_\parallel}$ are the total scattering rates between the states $k_\parallel$ and $k'_\parallel$. Note that no spin selection has been introduced in the model since all the experiments have been performed without polarization selection. We assume that cylindrical symmetry holds for the reciprocal

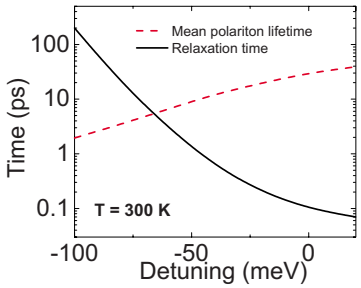

FIG. 4. (Color online) Relaxation time (black solid line) and mean polariton lifetime given by Eq. (2) (red dashed line) as a function of detuning. At $\delta \sim -65$ meV, the crossing of the lifetime and the relaxation time corresponds approximately to the critical value where the system enters the thermodynamic regime at $T = 300$ K.

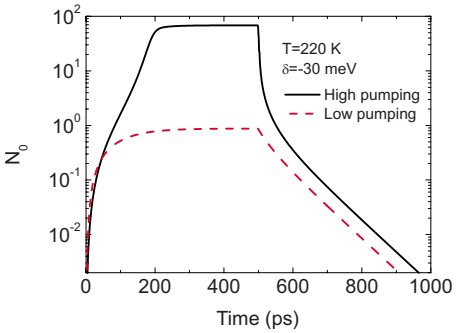

FIG. 5. (Color online) Dynamics of the occupation of the ground state $N_0(t)$ below and above threshold at 220 K for a detuning of −30 meV.

space at all times considered but wave-vector conservation in the 2D reciprocal space is properly accounted for in each scattering process. The scattering rates are calculated using Fermi's golden rule, which includes exciton-phonon, exciton-exciton, and exciton-electron interactions. We account for the main interaction mechanisms of excitons with phonons in GaN, namely,[49] Fröhlich interaction (which involves LO phonons), and deformation-potential and piezoelectric interactions (which involve acoustic phonons). The exciton-exciton and exciton-electron interactions have been treated in the Born approximation. The following parameters have been considered for the calculations: effective electron and heavy-hole masses $m_e = 0.2m_0$ and $m_h = 1.1m_0$,[50] with m_0 the free-electron mass, exciton binding energy $E_b = 49$ meV,[28] bulk exciton Bohr radius $a_B = 3.2$ nm, effective refractive index $n = 2.6$, LO-phonon energy $E_{\mathrm{LO}} = 92$ meV, deformation potential $D = 11.1$ eV,[49] mass density $\rho = 6150$ kg/m^3, speed of sound (in the [0001] direction) $c_s = 7960$ m/s,[51] inhomogeneous broadening $d = 25$ meV, cavity photon lifetime $\tau_c = 0.2$ ps, and a Rabi splitting $\Omega = 56$ meV. The expression for the matrix element of paraexciton interaction and that for the matrix element of exciton-electron interaction in the Born approximation were taken from Ref. 52. As a first approximation, the exciton nonradiative lifetime is considered to be independent of the temperature and taken equal to 50 ps. The main weakness of the Boltzmann approach is that it neglects the renormalization of the polariton dispersion arising from particle-particle interactions.[53] The simulation results are therefore expected to be quite reliable below threshold and for the determination of the threshold value. This determination becomes even more precise when the threshold value is not too large (i.e., when renormalization effects are still weak). Above threshold, this kind of modeling is formally not valid anymore but it can still give interesting information.

Figure 4 shows a typical example of information which can be extracted from Boltzmann simulations of polariton relaxation. Here, we assume that the nonresonant pumping scheme induces the generation of an exciton gas following a Bose distribution function with an effective temperature given by the LO-phonon energy (i.e., $T \sim 1070$ K). The pumping can be assumed to be either pulsed so that an initial distribution is introduced in the system at $t = 0$, and then freely evolves with time, or cw so that particles are generated at a constant rate. In order to calculate the relaxation time τ_{rel} of the exciton-polariton gas, we have considered the pulsed excitation case with an infinite polariton lifetime. The relaxation time is defined as the characteristic time of the temperature decay, which can be measured experimentally.[49] When calculating τ_{rel} this way, it can be linked with the signal rise time of the cavity emission in pulsed experiments carried out with short ps pulses. Figure 4 shows the evolution of τ_{pol} and τ_{rel} versus exciton-photon detuning at 300 K. As expected, the relaxation time is much longer than the mean polariton lifetime at large negative detunings. The system is therefore expected to be strongly out of equilibrium, i.e., in the so-called kinetic regime. The two curves cross at $\delta \sim -65$ meV and the lifetime becomes much longer than the cooling time when approaching positive detunings, which means that the system is in the so-called thermodynamic regime in this detuning range.

Figure 5 shows the calculated occupation of the ground state $N_0(t)$ for two different pumping powers, below and above threshold at a detuning of −30 meV at $T = 220$ K. Below threshold, the rise time is quite long and a real steady-state regime is only achieved at the end of the 500 ps of the pulse duration. Above threshold, the dynamics becomes much faster and the rise time becomes shorter and shorter when increasing the pumping power. After the end of the exciting pulse, $N_0(t)$ decays with a decay time given by the mean particle lifetime defined in Eq. (2) and in the low pumping regime (dashed red curve), the distribution function is Boltzmann type. In the high pumping regime, the distribution function is Bose type, with a large occupation of the ground state. The mean lifetime is therefore shorter until the ground-state occupation reaches unity where the system recovers its low pumping-regime characteristics.

Figure 6 shows the plot of the kinetic distribution function after 50 ps, when the emission from the cavity is still rising, and at 500 ps, when a steady-state regime is achieved below (solid) and above (dashed) threshold. The calculation is performed for a lattice temperature of 220 K. The effective temperature of the gas in the range of excess energy 20–100 meV is about 260 K as shown by the green dashed curve. Closer to the ground state, the distribution function is weakly depleted. Using only the range 0–15 meV of excess energy, we can deduce an effective temperature of 350 K for the

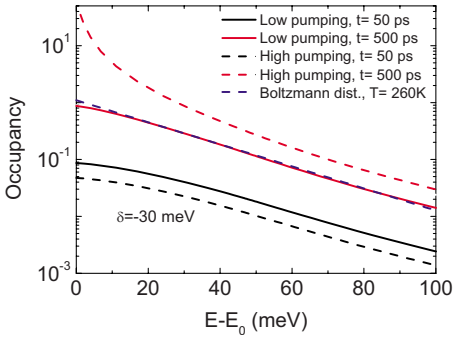

FIG. 6. (Color online) Occupancy of the polariton states at $\delta=-30$ meV and $T=220$ K below (solid) and above (dashed) threshold at two different times (50 ps, black and 500 ps, red) under quasi-cw excitation (500 ps long pulses). The blue dashed curve is a Boltzmann fit of the red curve with an effective temperature found equal to 260 K. E_0 corresponds to the lowest-energy state of the system.

polariton gas. It is also interesting to notice that polaritons close to $k_{\|}=0$ are warmer in the transient regime ($t=50$ ps) with an effective temperature close to 500 K.

IV. 2D POLARITON CONDENSATION PHASE DIAGRAMS: EXPERIMENT AND THEORY

In this section, we compare experimental and theoretical results mainly showing the threshold power dependence of cavity polariton condensation—when using incoherent optical pumping—on two independent tunable parameters that are exciton-cavity photon detuning (covering the −120 to −10 meV range) and lattice temperature (covering the 4–340 K range). As both of them will act differently on P_{thr}, a deeper understanding of the underlying physics governing the formation of polariton condensates is expected.

An important aspect related with the measurements of P_{thr} deals with the regime that can be reached by the polariton gas at the condensation threshold, namely, whether the system lies in the kinetic, the thermodynamic, or in an intermediate regime when polariton condensation takes place. Indeed, it allows establishing the distinction between a polariton laser and a Bose-Einstein condensate of polaritons (i.e., in the latter case, a system dominated by the thermodynamics) for the present system. A detailed qualitative picture of the transition between kinetic and thermodynamic regimes has been given in Sec. III B. Note once again that it is understood that the main criteria defining a polariton laser are fulfilled by a polariton BEC but the reverse is not true. We therefore performed angular-resolved PL measurements at threshold to check whether a reasonable equilibrium of the polariton gas with the lattice can be observed in the present system, i.e., we need to demonstrate that the MQW GaN MC can exhibit a temperature *relatively* close to that of the lattice at threshold. Measurements shown in Figs. 7(a)–7(c) have been carried out at $T_{latt}=220$ K and a detuning of −30 meV. The aim of these measurements consists in showing that the thermodynamic regime can be reached with the present sample in the high-temperature regime, i.e., when the threshold becomes temperature dependent at a given detuning.[14,31,32] The dispersion curve measured at threshold is displayed in Fig. 7(a) together with fits deduced from a standard coupled oscillator model. As previously reported, the polariton system exhibits a reduced normal-mode splitting of ~40 meV due to the blueshift of the LPB and the redshift of the UPB.[32] It is also seen that the upper energy states at low in-plane wave vectors lie at the energy of the renormalized uncoupled exciton mode. This could be due to the fact that in the high-density regime some quantum wells are not efficiently coupled with the cavity mode (indeed due to the peculiar geometry of the present sample the wells are not all positioned at a field antinode)[28] so that the emitted PL corresponding to these states could originate from uncoupled excitonic states. The relative polariton population of the LPB as a function of the emission energy is reported in Fig. 7(b). It is derived using the standard procedure which consists of a correction of the integrated PL intensity at a given angle (equivalently in-plane wave vector) by the corresponding photon fraction as previously shown in, e.g., Ref. 48. In this particular case, an effective temperature $T_{eff,\mathrm{LPB}}=500\pm30$ K, which is less than the exciton binding energy,[28] can be assigned to the polariton gas when using a Boltzmann-type exponential decay of the distribution function. Note that the measured excess temperature is larger than the theoretical one ($T=350$ K). However, this demonstrates the onset of the thermodynamic regime. At first sight, the excess temperature could seem fairly high. However, one should keep in mind that the present experiments are carried out with an initial carrier population with a large excess kinetic energy (~1 eV as quoted above). Note also that the relative difference between effective and lattice temperatures $(T_{eff,\mathrm{LPB}}-T_{latt})/T_{latt}=127\%$ is comparable or even lower than that observed in other MC systems where polariton BEC has been reported.[10,11,14] Since we also have access to the states of the upper branch, it is of interest to determine the effective temperature of those states. Here we assume that the low in-plane wave-vector states belong to the upper polariton branch [even though we observe a deviation to the calculated dispersion curve derived from the coupled oscillator model, Fig. 7(a)]. The correction of the integrated PL intensity by the photon fraction of upper polariton states leads to a polariton distribution characterized by an effective temperature $T_{eff,\mathrm{UPB}}=220\pm35$ K, which is equal to that of the lattice. The difference observed between $T_{eff,\mathrm{LPB}}$ and $T_{eff,\mathrm{UPB}}$ could originate from a more efficient coupling of upper polariton states to the exciton reservoir which should be fully thermalized.

Since the threshold corresponds to a transition between two phases (the condensed and uncondensed phases), we can display figures that can be identified with cross sections of the 3D phase diagram displayed in Ref. 32 [2D plots such as (δ, P_{thr}) and (T_{latt}, P_{thr}) curves]. Figure 8 shows the experimental threshold power dependence on temperature [Fig. 8(a)] and detuning [Fig. 8(b)]. For the available detuning range, a nonlinear decrease in P_{thr} is observed at low temperatures when going toward positive detunings. This is a direct manifestation of the kinetic regime, the radiative polariton lifetime being shorter than the relaxation time due to the dominant photonic fraction of $k_{\|}=0$ lower polariton

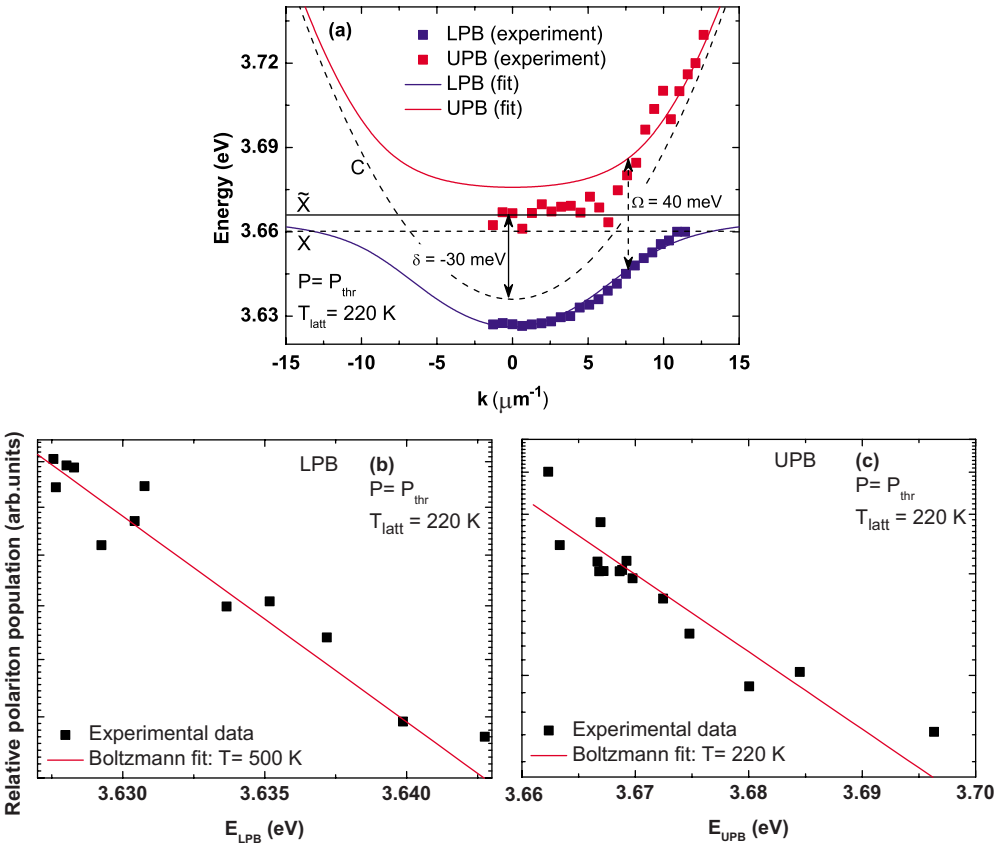

FIG. 7. (Color online) (a) Dispersion curve extracted from angular-resolved PL experiments performed at $T=220$ K at threshold for a detuning $\delta=-30$ meV. Fits of the polariton branches deduced from a coupled oscillator model as well as the position of the uncoupled cavity mode (C) and that of the uncoupled exciton mode before (X) and after renormalization ($\tilde{X}$) are also reported. Relative polariton population (i.e., integrated PL intensity corrected for the photon fraction of the states involved) as a function of the peak energy for (b) the LPB and (c) the UPB corresponding to the dispersion curve displayed in (a) (see text for details).

states. For intermediate temperatures ($T_{latt}\sim 150-300$ K), P_{thr} first decreases and then starts increasing again when going toward positive δ values [Fig. 8(b)]. In this temperature range, the threshold power can be minimized, i.e., an optimum detuning corresponding to a balance between polariton relaxation time and radiative lifetime can be found. For $\delta > \delta_{opt}$, polaritons are thermalized and the threshold is controlled by the thermodynamic properties of the system whereas for $\delta < \delta_{opt}$, polaritons are not thermalized and the threshold is controlled by the kinetics. For even higher temperatures, the optimum detuning goes out of the range of experimental measurements and in the whole (δ, T_{latt}) range we observe the thermodynamic regime, with the threshold power density increasing with detuning because of the joint

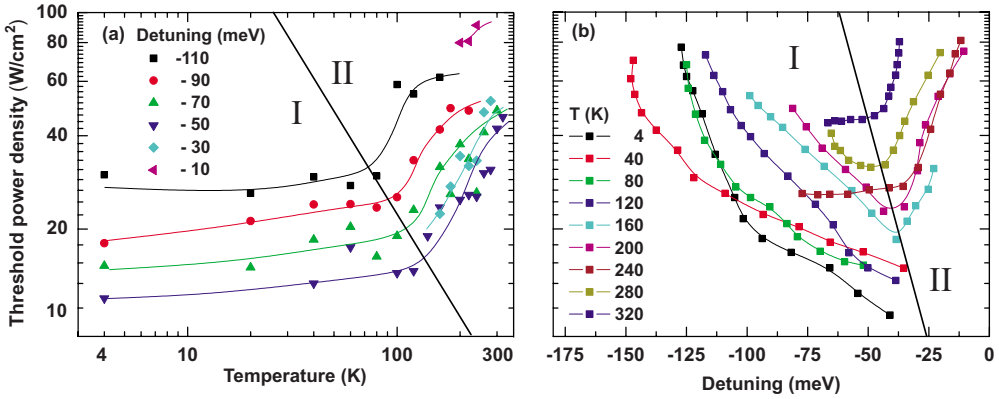

FIG. 8. (Color online) Experimental threshold power density as a function of (a) lattice temperature at various detunings (lines are a guide for the eyes) and (b) detuning at various temperatures. Region (I) corresponds to a kinetically driven system whereas (II) corresponds to a thermodynamic-like behavior.

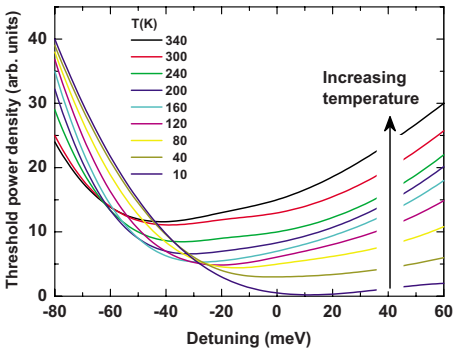

FIG. 9. (Color online) Theoretical dependence of the threshold power density as a function of detuning at various temperatures (see text for details).

increase in the effective mass[54] and the thermal escape of polaritons from the bottom of the trap toward LPB states beyond the inflection point.[32,55] Note also that at a given temperature, the more negative the detuning, the larger P_{thr} until thermal escape of lower polaritons starts playing a role for detunings closer to zero [Fig. 8(a), $\delta=-30$ and -10 meV]. This is the opposite behavior with respect to the prediction for a system operating in the exact thermodynamic limit [Fig. 2(a)], which can certainly be ascribed to relaxation kinetic effects.

These results are well reproduced by theoretical simulations performed using semiclassical Boltzmann equations. Contrary to the conditions for the calculation of the relaxation time shown in Fig. 4, we have adopted the same pumping scheme as in the experiment, i.e., a long quasi-cw pulse of 500 ps. Figure 9 displays the calculated threshold power density as a function of detuning for different temperatures. An important feature of these curves is that they cross. To be more precise, the higher the temperature, the larger the threshold in the thermodynamic regime (region corresponding to slightly negative and positive detunings) whereas the higher the temperature, the lower the threshold in the kinetic regime. Therefore those curves will cross as it was recently reported for CdTe- and GaAs-based MC samples on a much narrower temperature range.[14,31] Such a crossing is however not systematically observed in the present experiment. We believe that in addition to thermal escape mechanisms this is due to the temperature dependence of the nonradiative exciton lifetime which is presently neglected in the theory. The nonradiative lifetime decreases versus T which therefore results in a slight rise of the threshold versus T.

In theoretical calculations, a wider range of detunings is accessible, which allows plotting δ_{opt} for a large range of temperatures. In Fig. 10(a), we thus compare $\delta_{opt}(T)$ deduced from experimental measurements to theoretical calculations. The general trend is a shift of the optimum detuning toward more negative δ values with increasing temperature. The green line is the experimental analog of the line $\delta_{opt}(T)$ sketched in Fig. 3(b). Based on the analysis of Fig. 3(b), we can extract from this line a critical escape temperature $T_{esc}=258\pm10$ K associated with an optimum detuning of ~ -45 meV beyond which the optimum polariton condensation threshold power strongly increases due to a large depletion of the fundamental LP state [see also Fig. 10(b)]. Interestingly enough, the corresponding thermal energy $E_{esc}=22$ meV does indeed coincide with the minimum energy required to scatter polaritons from the bottom of the trap to LPB states beyond the inflection point for a renormalized normal-mode splitting of ~ 40 meV.[32,55] As quoted in Sec. III C, the difference observed between theory (solid red line) and experiment (circles) might stem from the fact that renormalization effects of the polariton dispersion curve are not taken into account when using the Boltzmann approach. At 300 K, the optimum value is about -53 meV. This is in sharp contrast with the expected behavior for a VCSEL, where the lowest threshold is obtained when the exciton (or electron-hole plasma) transition is resonant with the cavity mode, namely, at zero detuning.[32,55,56] The peculiar asymmetric shape of the condensation phase diagram and especially the existence of a nontrivial optimum detuning for each temperature is thus a direct signature of the matter-side of polaritons.

Another quantity which can be advantageously plotted is the evolution of the threshold power at the optimum detuning δ_{opt} versus temperature [Fig. 10(b)]. P_{thr} increases with temperature in both theory and experiment, which is likely originating from the increase in the thermodynamic threshold with temperature. The latter will slightly prime over the

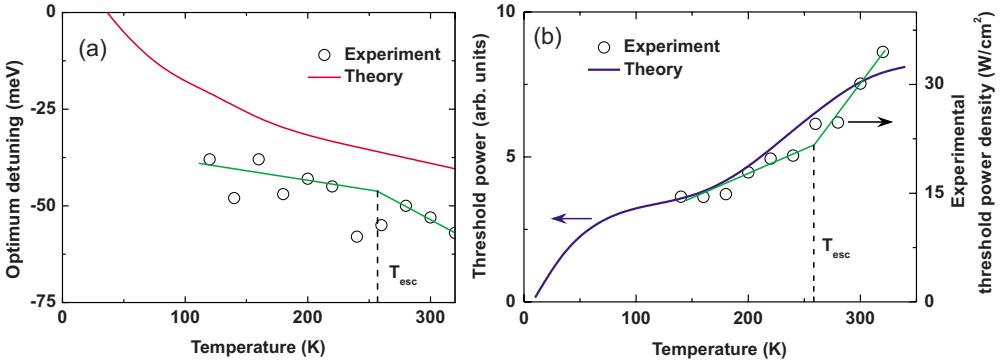

FIG. 10. (Color online) (a) Optimum detuning as a function of lattice temperature [experiment (circles) and theory (solid red line)]. The green line is a guide for the eyes plotted in connection with the line $\delta_{opt}(T)$ sketched in Fig. 3(b) (see text for details). (b) Condensation threshold power at the optimum detuning as a function of lattice temperature [experiment (circles) and theory (solid blue line)]. The green line is a guide for the eyes plotted in connection with the guide for the eyes of Fig. 10(a) (see text for details).

threshold given by the kinetics in this intermediate region (cf. Sec. III B.). Note however that the situation might be different in other systems, where the enhancement of kinetics with temperature, e.g., at cryogenic temperatures, might play a stronger role.[14,31] Finally, as for the evolution of $\delta_{opt}(T)$, we can define two slopes for the evolution of the optimum condensation threshold power as a function of T [green line in Fig. 10(b)] with the kink occurring at the same critical temperature $T_{esc}=258\pm10$ K, which would coincide with the appearance of significant depletion effects of the fundamental LP state.

V. CONCLUSION

In conclusion, the phase diagram of polariton condensation occurring in a MQW GaN-based MC has been analyzed theoretically and experimentally as a function of two independent parameters that are exciton-cavity photon detuning and temperature, which can be tuned over unprecedented ranges. In particular, for most of the accessible lattice temperatures, an optimum threshold has been found where the system switches from a kinetically (at large negative detunings and/or low cryogenic temperatures) to a thermodynamically driven condensation threshold (close to zero detuning and at high temperatures). It corresponds to the situation where the system fulfils a trade-off for two opposite constraints, namely, the antagonist evolution of the kinetic and thermodynamic thresholds. This kinetic to thermodynamic transition divides the phase diagram into two parts and the corresponding position $\delta_{opt}(T)$ in the (δ,T) plane corresponds to the minimum condensation threshold power. It therefore defines the optimum region where a polariton laser should operate. Contrary to a VCSEL where $\delta_{opt}(T)$ is expected to be *a priori* pinned to zero detuning for all temperatures, the situation appears to be strongly different for a polariton laser/condensate. Both experiment and theory indicate a progressive shift of $\delta_{opt}(T)$ toward more negative δ values when the temperature increases. This explains the singular shape of the phase diagram. The existence of a temperature-dependent optimum detuning leading to condensation is directly inherited from the dual light-matter nature of polaritons since the threshold is essentially driven by the efficiency of the various polariton relaxation channels [that in turn depend on detuning (due to a change in the exciton/photon fraction) and lattice temperature (due to a modification of the weight of polariton-polariton and polariton-phonon interactions)]. At high temperatures, polariton detrapping effects from the bottom of the trap formed in $k_{\|}$ space by the lower polariton branch are also found to play a supplementary role among the processes governing the condensation threshold. Finally, it has also been experimentally verified that the polariton gas in the thermodynamic-like region of the condensation phase diagram, though being thermalized, exhibits an excess temperature compared to that of the lattice as predicted by the theory.

ACKNOWLEDGMENTS

This work was supported by the EU project Stimscat, by the NCCR Quantum Photonics, research instrument of the Swiss National Science Foundation, and by the FNS under Grant No. 200020-122294.

[1] O. Penrose and L. Onsager, Phys. Rev. **104**, 576 (1956).
[2] P. C. Hohenberg, Phys. Rev. **158**, 383 (1967).
[3] J. M. Kosterlitz and D. J. Thouless, J. Phys. C: Solid State Phys. **6**, 1181 (1973).
[4] D. R. Nelson and J. M. Kosterlitz, Phys. Rev. Lett. **39**, 1201 (1977).
[5] D. S. Fisher and P. C. Hohenberg, Phys. Rev. B **37**, 4936 (1988).
[6] P. Kapitza, Nature (London) **141**, 74 (1938).
[7] D. J. Bishop and J. D. Reppy, Phys. Rev. Lett. **40**, 1727 (1978); Phys. Rev. B **22**, 5171 (1980).
[8] T. Nikuni, M. Oshikawa, A. Oosawa, and H. Tanaka, Phys. Rev. Lett. **84**, 5868 (2000).
[9] S. O. Demokritov, V. E. Demidov, O. Dzyapko, G. A. Melkov, A. A. Serga, B. Hillebrands, and A. N. Slavin, Nature (London) **443**, 430 (2006).
[10] M. Richard, J. Kasprzak, R. André, R. Romestain, L. S. Dang, G. Malpuech, and A. Kavokin, Phys. Rev. B **72**, 201301(R) (2005); J. Kasprzak, M. Richard, S. Kundermann, A. Baas, P. Jeambrun, J. M. J. Keeling, F. M. Marchetti, M. H. Szymańska, R. André, J. L. Staehli, V. Savona, P. B. Littlewood, B. Deveaud, and L. S. Dang, Nature (London) **443**, 409 (2006).
[11] R. Balili, V. Hartwell, D. Snoke, L. Pfeiffer, and K. West, Science **316**, 1007 (2007).
[12] S. Christopoulos, G. Baldassarri Höger von Högersthal, A. J. Grundy, P. G. Lagoudakis, A. V. Kavokin, J. J. Baumberg, G. Christmann, R. Butté, E. Feltin, J.-F. Carlin, and N. Grandjean, Phys. Rev. Lett. **98**, 126405 (2007).
[13] G. Christmann, R. Butté, E. Feltin, J.-F. Carlin, and N. Grandjean, Appl. Phys. Lett. **93**, 051102 (2008).
[14] J. Kasprzak, D. D. Solnyshkov, R. André, L. S. Dang, and G. Malpuech, Phys. Rev. Lett. **101**, 146404 (2008).
[15] A. V. Kavokin, J. J. Baumberg, G. Malpuech, and F. P. Laussy, *Microcavities* (Oxford University Press, Oxford, 2007).
[16] M. G. A. Bernard and G. Durrafourg, Phys. Status Solidi **1**, 699 (1961).
[17] Y. Yamamoto, S. Machida, and G. Björk, Phys. Rev. A **44**, 657 (1991); G. Björk, H. Heitmann, and Y. Yamamoto, *ibid.* **47**, 4451 (1993).
[18] C. Weisbuch, M. Nishioka, A. Ishikawa, and Y. Arakawa, Phys. Rev. Lett. **69**, 3314 (1992).
[19] A. Imamoglu, R. J. Ram, S. Pau, and Y. Yamamoto, Phys. Rev. A **53**, 4250 (1996).
[20] L. S. Dang, D. Heger, R. André, F. Bœuf, and R. Romestain, Phys. Rev. Lett. **81**, 3920 (1998).
[21] P. G. Savvidis, J. J. Baumberg, R. M. Stevenson, M. S. Skolnick, D. M. Whittaker, and J. S. Roberts, Phys. Rev. Lett. **84**, 1547 (2000); R. M. Stevenson, V. N. Astratov, M. S. Skolnick, D. M. Whittaker, M. Emam-Ismail, A. I. Tartakovskii, P. G. Savvidis,

J. J. Baumberg, and J. S. Roberts, *ibid.* **85**, 3680 (2000).
[22] D. Bajoni, P. Senellart, E. Wertz, I. Sagnes, A. Miard, A. Lemaître, and J. Bloch, Phys. Rev. Lett. **100**, 047401 (2008).
[23] G. Malpuech, A. Di Carlo, A. Kavokin, J. J. Baumberg, M. Zamfirescu, and P. Lugli, Appl. Phys. Lett. **81**, 412 (2002).
[24] M. Zamfirescu, A. Kavokin, B. Gil, G. Malpuech, and M. Kaliteevski, Phys. Rev. B **65**, 161205(R) (2002).
[25] F. Semond, I. R. Sellers, F. Natali, D. Byrne, M. Leroux, J. Massies, N. Ollier, J. Leymarie, P. Disseix, and A. Vasson, Appl. Phys. Lett. **87**, 021102 (2005).
[26] R. Butté, G. Christmann, E. Feltin, J.-F. Carlin, M. Mosca, M. Ilegems, and N. Grandjean, Phys. Rev. B **73**, 033315 (2006).
[27] J. J. Baumberg, A. V. Kavokin, S. Christopoulos, A. J. D. dy, R. Butté, G. Christmann, D. D. Solnyshkov, G. Malpuech, G. Baldassarri Höger von Högersthal, E. Feltin, J.-F. Carlin, and N. Grandjean, Phys. Rev. Lett. **101**, 136409 (2008).
[28] G. Christmann, R. Butté, E. Feltin, A. Mouti, P. A. Stadelmann, A. Castiglia, J.-F. Carlin, and N. Grandjean, Phys. Rev. B **77**, 085310 (2008).
[29] D. Solnyshkov, H. Ouerdane, and G. Malpuech, J. Appl. Phys. **103**, 016101 (2008).
[30] δ is set as the energy difference at zero in-plane wave vector ($k_{\|}=0$) between the position of the uncoupled cavity mode *C* and that of MQW excitons *X*.
[31] E. Wertz, L. Ferrier, D. D. Solnyshkov, P. Senellart, D. Bajoni, A. Miard, A. Lemaître, G. Malpuech, and J. Bloch, Appl. Phys. Lett. **95**, 051108 (2009).
[32] R. Butté, J. Levrat, G. Christmann, E. Feltin, J.-F. Carlin, and N. Grandjean, Phys. Rev. B **80**, 233301 (2009).
[33] D. Porras and C. Tejedor, Phys. Rev. B **67**, 161310(R) (2003).
[34] J. Kasprzak, M. Richard, A. Baas, B. Deveaud, R. André, J.-Ph. Poizat, and L. S. Dang, Phys. Rev. Lett. **100**, 067402 (2008).
[35] V. Savona, in *Confined Photon Systems, Fundamentals and Applications*, edited by H. Benisty, J.-M. Gérard, R. Houdré, J. Rarity, and C. Weisbuch (Springer, Berlin, 1999), p. 172.
[36] R. W. Martin, P. G. Middleton, K. P. O'Donnell, and W. Van der Stricht, Appl. Phys. Lett. **74**, 263 (1999).
[37] D. Brunner, H. Angerer, E. Bustarret, F. Freudenberg, R. Höpler, R. Dimitrov, O. Ambacher, and M. Stutzmann, J. Appl. Phys. **82**, 5090 (1997).
[38] J.-F. Carlin and M. Ilegems, Appl. Phys. Lett. **83**, 668 (2003).
[39] J.-F. Carlin, C. Zellweger, J. Dorsaz, S. Nicolay, G. Christmann, E. Feltin, R. Butté, and N. Grandjean, Phys. Status Solidi B **242**, 2326 (2005).
[40] G. Malpuech, Y. G. Rubo, F. P. Laussy, P. Bigenwald, and A. V. Kavokin, Semicond. Sci. Technol. **18**, S395 (2003).
[41] G. Malpuech, D. D. Solnyshkov, H. Ouerdane, M. M. Glazov, and I. Shelykh, Phys. Rev. Lett. **98**, 206402 (2007).
[42] G. Christmann, D. Simeonov, R. Butté, E. Feltin, J.-F. Carlin, and N. Grandjean, Appl. Phys. Lett. **89**, 261101 (2006).
[43] A more accurate picture of such a diagram would include the temperature dependence of the static dielectric constant [cf., e.g., S. Shokhovets, O. Ambacher, B. K. Meyer, and G. Gobsch, Phys. Rev. B **78**, 035207 (2008)]. It would affect the determination of the Bohr radius and thus the exciton saturation density. In such a case, the horizontal line in Fig. 2(a) would exhibit a slightly negative slope.
[44] M. S. Skolnick, T. A. Fisher, and D. M. Whittaker, Semicond. Sci. Technol. **13**, 645 (1998).
[45] Jagdeep Shah, *Ultrafast Spectroscopy of Semiconductors and Semiconductor Nanostructures*, 2nd enlarged ed. (Springer-Verlag, Berlin, 1999), Chap. 6.
[46] Such a feature has been clearly evidenced, e.g., in single GaAs/AlGaAs quantum-well structures in M. Gurioli, A. Vinattieri, J. Martinez-Pastor, and M. Colocci, Phys. Rev. B **50**, 11817 (1994).
[47] F. Tassone, C. Piermarocchi, V. Savona, A. Quattropani, and P. Schwendimann, Phys. Rev. B **56**, 7554 (1997).
[48] A. I. Tartakovskii, M. Emam-Ismail, R. M. Stevenson, M. S. Skolnick, V. N. Astratov, D. M. Whittaker, J. J. Baumberg, and J. S. Roberts, Phys. Rev. B **62**, R2283 (2000).
[49] See, e.g., X. B. Zhang and B. Gil, in *Low-Dimensional Nitride Semiconductors*, edited by B. Gil (Oxford University Press, Oxford, 2002).
[50] M. Suzuki, T. Uenoyama, and A. Yanase, Phys. Rev. B **52**, 8132 (1995).
[51] R. Truell, C. Elbaum, and B. B. Chick, *Ultrasonic Methods in Solid State Physics* (Academic, New York, 1969).
[52] A. Kavokin and G. Malpuech, *Cavity Polaritons*, Thin Films and Nanostructures Vol. 32 (Elsevier, San Diego, 2003).
[53] C. Ciuti, P. Schwendimann, B. Deveaud, and A. Quattropani, Phys. Rev. B **62**, R4825 (2000).
[54] From very negative detunings up to zero detuning, the effective mass of polaritons lying at the bottom of the trap only changes by a factor of 2 with respect to the mass of cavity photons m_{ph}. Its impact on condensation will therefore play a role essentially for positive values when its increase will be several times larger than m_{ph}.
[55] J. Levrat, R. Butté, G. Christmann, E. Feltin, J.-F. Carlin, and N. Grandjean, Phys. Status Solidi C **6**, 2820 (2009).
[56] K. D. Choquette and K. M. Geib, in *Vertical-Cavity Surface-Emitting Lasers*, edited by C. Wilmsen, H. Temkin, and L. A. Coldren (Cambridge University Press, Cambridge, 1999), p. 199.